On-Demand Inkjet Printed Hydrophilic Coatings for Flow Control in 3D-Printed Microfluidic Devices Embedded with Organic Electrochemical Transistors

Anatolii Makhinia, Pooya Azizian, Valerio Beni, Jasmina Casals-Terré, Joan M. Cabot, and Peter Andersson Ersman**

A. Makhinia, V. Beni, P. Andersson Ersman
RISE Research Institutes of Sweden
Digital Systems, Smart Hardware, Printed, Bio- and Organic Electronics, Norrköping, Sweden
E-mail: peter.andersson.ersman@ri.se
A. Makhinia
Laboratory of Organic Electronics, Department of Science and Technology, Linköping University, Norrköping, Sweden
P. Azizian, J. M. Cabot
Energy and Engineering Department, Leitat Technological Center, Terrassa (Barcelona), Spain
E-mail: jmcabot@leitat.org
P. Azizian, J. Casals-Terré
Mechanical Engineering Department, Technical University of Catalonia, Terrassa (Barcelona), Spain

Keywords: 3D-printing; capillary-driven microfluidics; inkjet printing; OECT; hydrophilic coating

Abstract

Microfluidic surface chemistry can enable control of capillary-driven flow without the need for bulky external instrumentation. A novel pondered non-homogeneous coating defines regions with different wetting properties on the microchannel walls. It changes the curvature of the liquid-air meniscus at various channel cross-sections and consequently leads to different capillary pressures, which is favorable in the strive towards automatic flow control. This is accomplished by the deposition of hydrophilic coatings on the surface of multi-level 3D-printed (3DP) microfluidic devices via inkjet printing, thereby retaining the surface hydrophilicity for at least 6 months of

storage. To the best of our knowledge, this is the first demonstration of capillary flow control in 3DP microfluidics enabled by inkjet printing. The method is used to create “stop” and “delay” valves to enable pre-programmed capillary flow for sequential release of fluids. To demonstrate further utilization in point-of-care sensing applications, screen printed organic electrochemical transistors are integrated within the microfluidic chips to sense, sequentially and independently from external actions, chloride anions in the 1-100 mM range. The results present a cost-effective fabrication method of compact, yet comprehensive, all-printed sensing platforms that allow fast ion detection (<60 s), including the capability of automatic delivery of multiple test solutions.

1. Introduction

Capillary-driven microfluidic devices take advantage of capillary forces to move liquids without using any external pumps or valves, this occurs due to the intermolecular forces of the liquid and the surrounding solid surface within the microfluidic device. Such microfluidics has paved the way for implementing lab tasks into point-of-care (POC) devices, independent from complex peripheral equipment.

Geometrical changes, such as a sudden expansion in the microchannel cross-section, can modify the forefront meniscus of the liquid-air interface and, consequently, the driving force of the capillary flow. So, it is used to obtain the desired flow control. Autonomous capillary-driven microfluidic devices having microchannels with varying geometries have been proposed in the literature, to enable pre-programmed immunoassays based on sequential delivery of bio-liquids and reagents.[1–6]

Besides utilizing the geometry to manage the air-liquid meniscus and control the capillary flow, the use of surface chemistry within microfluidics can be exploited for spontaneous manipulation of liquids. Different microfluidic coatings lead to various liquid-solid contact angles. It changes the curvature of the liquid-air meniscus in various sections. Consequently, different capillary pressures are accessible at different stages. Zhao, *et al.*, formed virtual walls by creating different surface free energies through patterning of the microchannels using two methods based on self-assembled monolayer (SAM) chemistry. The first method created multi-stream liquid laminar flows (octadecyltrichlorosilane solution in hexadecane) to deposit SAMs on the microchannel sides. The areas where the silane solution stream passed were modified with SAMs and became hydrophobic, while areas where the non-silane solution stream passed remained hydrophilic. This

method requires pre-formed channels to drive multi-stream laminar flows, limiting the possible final patterns. The second method relied on a two-step process, where the whole surface of channels was first modified with photocleavable SAMs (2-nitrobenzyl), followed by ultraviolet (UV) irradiation of the microchannels to create hydrophilic patterns via photomasks.[7,8] UV irradiation through the masks on top of SAM-modified channels produced hydrophilic carboxylate groups in the exposed areas forming complex patterns. Furthermore, photolithography or dispensing (plotter pen) of hydrophilic patterns on hydrophobic surfaces as well as hydrophobic patterns on hydrophilic surfaces were performed to confine liquids into channels instead of limiting them by walls.[9,10]

The dominant materials used for the fabrication of microfluidic devices, like resin in 3D-printing (3DP) and polydimethylsiloxane (PDMS) in soft lithography, are poorly hydrophilic or hydrophobic, while hydrophilic interfaces (water contact angles of ≤60°) are needed to satisfy the required surface energy of such capillary microfluidics within water-based applications.[1] By treating these polymers with solely oxygen/air plasma and additionally with polyethylene glycol (PEG) or polyvinyl alcohol (PVA), hydrophilic surfaces are created by the introduction of polar functional groups containing oxygen, etc. However, the surface characteristics are gradually lost towards the initial state within a few hours of aging.[11] On the other hand, the polar functional groups introduced by plasma treatment provide suitable adhesion of any subsequently deposited coating.[12] Therefore, different coatings were considered to increase and keep the stability of the hydrophilic surface for a longer period. Hydrophilic PDMS-based microfluidics can be obtained by the deposition of PVA and polyethylene glycol PEG before and after plasma treatment, at the cost of additional processing steps.[13,14]

Digital printing technology, more precisely inkjet printing, has been employed for paper-based microfluidics by creating 2D structures (hydrophobic boundaries) on paper and by inkjet-etching of hydrophobic substrates. Moreover, inkjet printing was used for level-by-level (several materials) fabrication of microfluidics with 3D features as well as printing of embedded sensors along with microfluidic channels in bilayer microfluidic chip platforms.[15-20]

The inkjet printing technology ensures a low cost, scalable, and material/energy (2.4 – 10 pL ink drop volume) efficient manufacturing approach. The major advantage in comparison with other printing techniques is explained by the digital printing process featuring low ink consumption, high resolution deposition (~30-40 µm), customizable on-demand shape and thickness of the printed

structures including a large selection of materials on a variety of substrates.[21,22] To the best of our knowledge, inkjet printing of hydrophilic coatings onto microchannels of stereolithography (SLA) 3DP microfluidics has not been explored till now.

This study suggests a one-step surface modification method via fast and low-cost inkjet printing of a PSS^-Na^+-based hydrophilic coatings (several layers) on the surface of the multi-level 3DP resin to enable flow control in complex capillary microfluidic devices. On the contrary to plasma treatment, or other methods (in combination), this approach allows the creation of on-demand surface hydrophilicity at the place of interest (*e.g.*, reservoirs, valves, etc.). The wetting properties of the inkjet printed coating inside the 3DP microfluidic channels retain for a long period of at least 6 months, see Figure S1a, Movie S1 and Movie S2 in the supporting information.

To demonstrate the potential of our 3DP capillary microfluidics with inkjet printed hydrophilic coatings, we integrated fully screen printed organic electrochemical transistors (OECTs) within the microfluidic devices, thereby forming an all-printed sensing platform. The integration of OECTs with a surface-directed microfluidic system, manufactured via photolithography and without the pre-programmed sequential release of liquids, has been previously reported.[23] In our work, the functionality of the coatings inside the 3DP multi-level microchannels was verified by sensing Cl^- anions in the 1-100 mM range by the screen printed OECTs. The OECT technology, possibly integrated within microfluidic devices, shows a great potential for printed logic circuits and various biosensor applications, *e.g.*, for quantitative testing of glucose, lactate, cholesterol, and label-free DNA biosensing.[24-30]

2. Results and Discussions

2.1 Microfluidic function

Capillary flow is driven by the capillary pressure gradient caused by the arc meniscus front. This meniscus is formed by the surface tension applied on the liquid-air interface, which comes from the balance of the liquid-surface adhesion and the liquid intermolecular cohesion. Two-phase meniscuses across the capillary circuit provide driving and/or retention capillary pressure along or against the capillary flow. The capillary pressure can be calculated by employing the Young-Laplace equation based on channel size and liquid contact angle with the surface.[31] In a closed rectangular microchannel, the capillary pressure can be obtained according to **Equation (1)**:[2,32]

$$P = -\gamma\left[\frac{\cos\theta_t + \cos\theta_b}{h} + \frac{\cos\theta_l + \cos\theta_r}{w}\right] \quad (1)$$

where γ and P is the surface tension of the liquid and the pressure, respectively. θ_t, θ_b, θ_l, and θ_r is the top, bottom, left and right water contact angle on the respective channel wall. h is the channel height and w is the channel width. According to Hagen–Poiseuille's law, the pressure drop (ΔP) due to viscous forces on the walls can be described using the flow rate (Q) and the fluidic resistance (R). In the case of a rectangular cross-section channel, R can be calculated using the length (L) of the microchannel by **Equation (2)**:

$$R = \frac{12\mu L}{h^3 w}\left[1 - 0.630\frac{h}{w}\right]^{-1} \quad (2)$$

$$\Delta P = QR \quad (3)$$

Considering Equation (1) and **Equation (3)**, the direction and the flow rate of a capillary flow can be calculated, and the flow can be pre-programmed based on the parameters that change the pressure and the resistances. The schematics in **Figure 1** illustrate the modified capillary-driven microfluidics with hydrophilic microchannels, including the detection site with an embedded OECT sensor device. **Figure 2** shows 3DP capillary circuits, whose functionality are based on pre-designed parameters such as channel dimensions and contact angles. Figure 2a shows the resulting force balance (capillary force - viscous force) on the liquid bulk. An arc meniscus front drives the liquid into a microchannel covered by a printed hydrophilic coating. Different deposition strategies can lead to different contact angles, and as a result, various flow patterns. Figure 2b depicts changes in contact angle when the PSS^-Na^+-based hydrophilic coating is deposited on a hydrophobic surface. These changes in contact angles lead to a different force balance. Figure 2c shows the force balance differences in two parallel channels, caused by the

printed coating that leads to retention or capillary flow. In channel 1, reaching the non-coated surface completely stopped the flow, while in channel 2, the same aqueous liquid flowed into the channel by the capillary force.

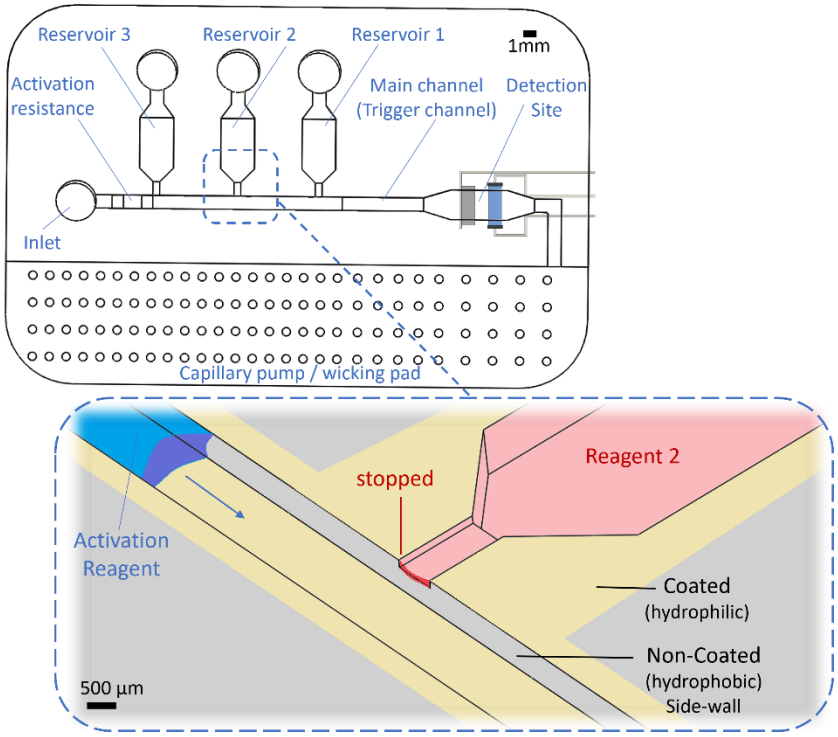

Figure 1. Schematics showing the 3DP capillary-driven microfluidics with pre-programmed delivery of liquid samples.

Altering the channel geometry by 3DP and the contact angle by the deposition of the coating allows for flow control. In analogy with electronic circuits, each two-phase meniscus can be represented as a potential source and the channels as resistances (Figure 2d). By applying Equation (1) and Equation (3) to calculate pressure (potential difference) and flow resistances, the sequential release of liquids can be pre-programmed (Figure 2e). As a result, the liquids from each reservoir (from 1 to 3) are released downstream towards the detection site and the capillary pump, where the flow rate is controlled by the suction power of the capillary pump and the sum of the flow resistances.

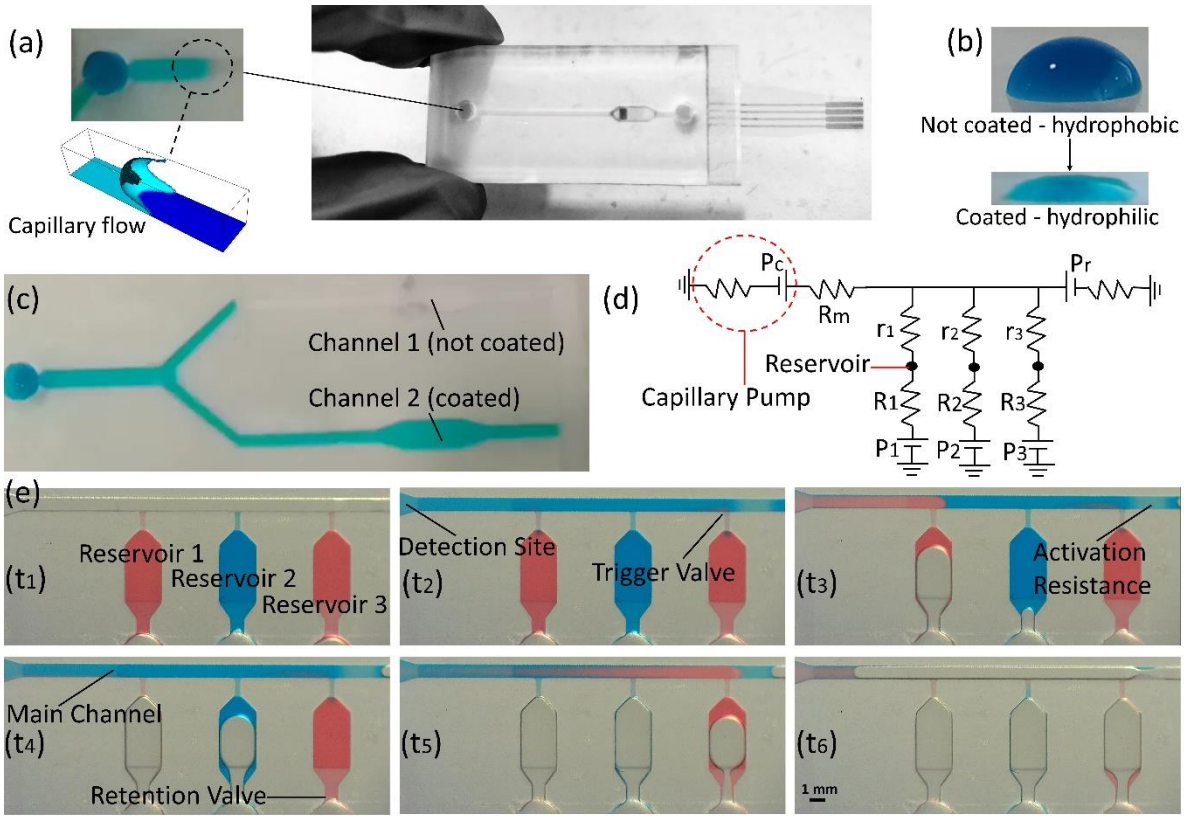

Figure 2. Capillary-driven microfluidics: a) Adhesion of liquid molecules to the coated hydrophilic surface forms a surface tension and a liquid-air meniscus to drive the liquid spontaneously through the microchannel. The capillary driving force can be changed by using different deposition strategies of the hydrophilic coating. b) Effect of the hydrophilic coating on the liquid-surface contact angle. c) Capillary flow fills the coated channel, but it stops at the edge of the non-coated microchannel. d) The equivalent electronic circuit of the capillary microchannels used for automatic sequential delivery of liquid samples. e) Pre-programmed delivery of liquid samples using capillary action based on the designed geometry of the microfluidics and the coating.

2.2 Ink formulation, inkjet printing conditions, wettability and stability of the coatings

Herein, the ink for coating was prepared by dissolving 15 wt% poly(sodium-4-styrene sulfonate) ($PSS^{-}Na^{+}$) in deionized water at ambient conditions, followed by the viscosity measurements to verify its suitability for inkjet printing. An ink viscosity of ~ 6.7 mPas was obtained, which falls within the range of the required viscosity for inkjet printing. It is well established that the ink and film properties can be improved by mixing a low boiling point solvent, being the main solvent,

with a high boiling point solvent as the co-solvent.[33] Therefore, the prepared solution was further optimized by adding 10 wt% of poly(ethylene glycol).

Physical properties, such as viscosity, substrate surface free energy and contact angle are crucial for the film formation on various substrates.[34] The mixture of water and poly(ethylene glycol) (90:10 wt% ratio) was employed to prevent clogging of the nozzle and fast evaporation of the ink at the nozzle-air interface.[35] The inkjet printing process was performed on quartz glass substrates and 3DP microfluidic chips to assess and compare printability. The inkjet printing on quartz glass and 3DP substrate was carried out by several subsequently printed layers at a print resolution of approximately 1000 dots per inch (DPI). A resulting coating thickness of 570 nm (and a minimum linewidth of 35 µm ± 5 µm) was obtained on quartz glass (Figure S2), while 3DP substrates resulted in non-homogeneous coatings (Figure S3). This could be explained by the high surface roughness of the 3DP substrate (>6 µm, which exceeds the thickness of the PSS^-Na^+-based coating) and its poor hydrophilicity. It is well known that the quartz glass has good wettability and low surface roughness. As a result (**Table 1**), the designed widths and the actual widths of the printed patterns on 3DP substrates (hydrophobic) and quartz microscope glass slides (hydrophilic) are differing, which is an indication of different surface properties.

Table 1. Comparison of the printability of the hydrophilic coatings on quartz glass and 3DP substrates.

15 wt% PSS^-Na^+-based coating:	**Ink printability: width [µm]**	
	400 (design)	600 (design)
on 3DP resin	375.7 ± 8.6	586.4 ± 3.2
on quartz glass	392.8 ± 8.9	609.1 ± 9.3

As already mentioned, the surface free energy, the contact angle of the substrate and the viscosity of the ink are important parameters that enable uniform and homogeneous film formation. To investigate the wettability of the 3DP resin and the PSS-Na+-based hydrophilic coating, the water contact angles of the two surfaces were measured. The deposited coating on the 3DP substrate resulted in reduction of the hydrophobicity (water contact angles changed from 69.7° ± 0.57 to 40.1° ± 7.85), see **Figure 3**. The measurements indicated a hydrophilic surface (good wetting) on the PSS-Na+-coated resin and a hydrophobic feature on the 3DP resin. The coating is mainly envisioned for single use, applicable in disposable sensor systems. The PSS-Na+ is water soluble,

which implies that the coating gradually dissolves over time, or absorbs moisture when stored at ambient conditions (22°C and 47RH%). The latter resulted in even lower water contact angle (~31°) after 12 days of storage, see Figure 3. The suitability of using inkjet printed coatings inside 3DP microfluidics for sensor systems was successfully assessed after 6 months of storage in a plastic bag, *i.e.*, the coating retained its surface hydrophilicity after long-term storage (Figure S1a, Movie S1, Movie S2).

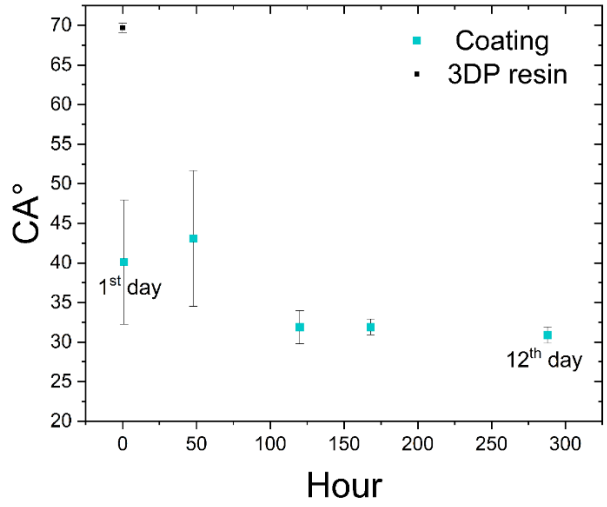

Figure 3. Change of water contact angle (CA°) as a function of time (hours) of coated and non-coated 3DP resin substrates stored at ambient conditions.

2.3 Inkjet printing of on-demand patterns

The drop-on-demand inkjet printing technology has the potential to expand the frontiers of 3DP capillary-driven microfluidics to modulate, for example, the release of fluids or their flow via so-called “stop” and “delay” valves that will be introduced in this section.

The inkjet printed polyelectrolyte coating on the surface of the 3DP resin, reported herein, reduces the contact angle and changes, in this way, the wetting behaviour of the resin-based substrate to hydrophilic, thereby making it suitable for capillary microfluidics. In **Figure 4**a, we show an on-demand inkjet printed pattern on quartz glass, including approximately 400 µm wide stripes without the coatings. As a step further, the printing was adapted for the deposition of the same coating pattern on the 3DP resin of a microfluidic chip.

The deposited printed array was designed to manipulate (stop or delay) the flow of the liquid (a water solution) inside various channels of microfluidic chips. In particular, the pattern deposited inside the microfluidic channel (Figure 4b and Figure 4d) comprised ~600 µm and ~800 µm coated

and non-coated alternating areas. The areas free from coatings were expected to delay (Figure 4b) or stop (Figure 4d) the flow inside the microfluidic system, thereby acting as "delay" (400-600 µm) or "stop" (>800 µm) valves. Figure 4c shows the implementation of the "stop" and "delay" valves in the 3DP microfluidic channels, where the respective valve is indicated by the brackets.

In Figure 4b and Figure 4d, the red arrows ("Additional printed margin" or "No margin") indicate areas introduced to simplify the inkjet printing process, *e.g.*, to avoid misalignment issues. Movie S3 and Movie S4 in the supporting information show the flow behaviour of the liquids in these microfluidic channels.

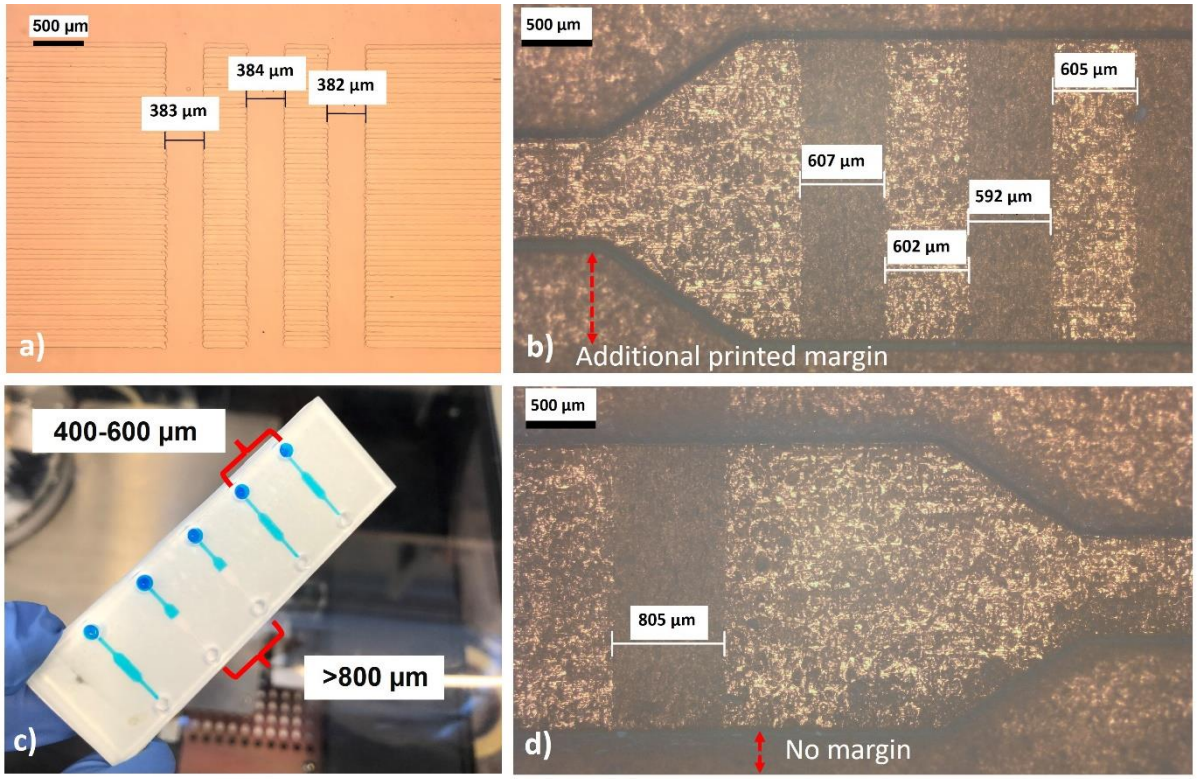

Figure 4. Inkjet printing of polyelectrolyte-based (PSS^-Na^+) on-demand patterns. A) Microscope image of inkjet printed coating on quartz glass with approximately 400 µm wide alternating coated and non-coated areas. B) Microscope image of inkjet printed patterns with approximately 600 µm alternating coated and non-coated areas inside the channel of the 3DP microfluidic device, intended to delay the flow. c) Demonstration (photograph) of modified microfluidic channels with approximately 600 µm and 800 µm alternating coated and non-coated areas. The image was taken after approximately 10 minutes of storage under ambient conditions. d) Microscope image with the 800 µm non-coated area (intended to terminate the flow).

2.4 Inkjet printing of hydrophilic coatings to enable capillary-driven microfluidics with automatic release of test solutions

Controlled release of test solutions has previously been demonstrated with capillary-driven microfluidics.[1,3,5] **Figure 5**a shows a schematic illustration and Figure 5b shows a photograph of a functional microfluidic device. For the sequential release of reagents, the device encompasses a reaction chamber, a capillary pump containing tissue paper, and three reservoirs (approximately 20 μL each) to keep solutions with different dilution of the reagents. The inkjet printed coating lowers the water contact angle inside the microchannels and enables the capillary flow, while the deliberated retention pressures at the reservoirs upstream take care of the sequential release of fluids (colored dyes).

In the work reported herein, the bottom channel walls of various crucial parts (including additional printed margin areas, see Figure 5c and Figure 5d) of the 3DP microfluidic chip were patterned with the inkjet printed hydrophilic coating to enable autonomous delivery of test solutions to the so-called reaction chamber, which is equipped with a sensing device. Because of the hydrophilic coating and the channel geometry, the automatic and sequential release of three fluids with colored dyes has been realized. The purple fluid was released first, as shown in Figure 5b (already in the reaction chamber), followed by the consecutive release of the red and the blue colored fluids, see also Movie S5 in the supporting information.

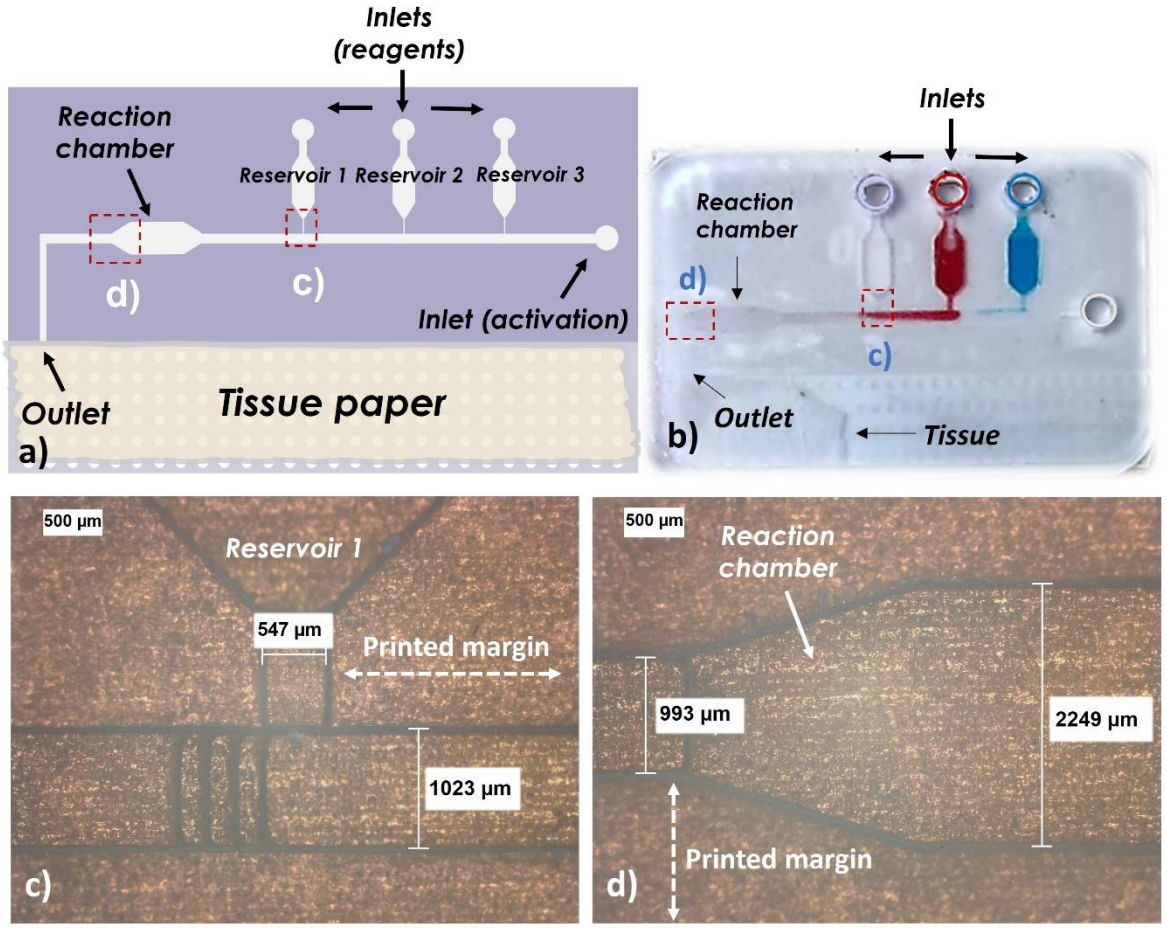

Figure 5. 3DP capillary-driven microfluidic chip including hydrophilic coatings (non-homogeneous). a) Schematic illustration and b) photograph of a microfluidic device during the sequential release of the colored dyes (purple is first, followed by red and finally blue). c) The connection between one of the test solution reservoirs and the common channel covered with the hydrophilic coating. d) Part of the sensing chamber with the inkjet printed coating. Movie S5 in the supporting information demonstrates the sequential release of the three test solutions in this microfluidic device.

2.5 Sensing of chloride anions by using an OECT-based sensor integrated in modified capillary-driven microfluidics

Figure 6a and Figure 6b show the use of the aforementioned microfluidic circuit for sensing applications, such as the sequential detection of multiple concentrations of Cl^- anions (1, 10 and 100 mM) with a screen printed OECT-based sensor; the OECT output and transfer characteristics at different ion concentrations are shown in Figure S4 in the supporting information. For this, current vs. time measurements were performed.[19] More specifically, the drain current (I_D) was recorded (the drain voltage, V_D, was kept constant at either -0.2 or -0.3 V) while the different

solutions, with subsequently increased concentration of Cl^- anions, were sequentially released and driven to the sensor. The I_D current was modulated due to the increasing concentration of Cl^- anions brought in contact with the sensing element (the Ag/AgCl gate electrode), as shown in Figure 6d and Figure 6e; the recorded response was in agreement with Nernst equation.[36] Once the automatic release was initiated, the OECT sensor was exposed to a 100 mM $NaNO_3$ buffer solution that served as the baseline for the following stepwise delivery of the 1, 10 and 100 mM NaCl solutions to the sensing chamber. The solution of each one of the NaCl concentrations was pre-mixed into a 100 mM $NaNO_3$ electrolyte buffer solution. To verify the results obtained with the microfluidic device, a set of experiments based on dropcasting of the analyte solutions on the sensor were performed, see Figure S5 in the supporting information.

A linear variation (as expected from the Nernst equation) in the sensor response was recorded (Figure 6e), for both experimental configurations, for increasing concentrations of Cl^- anions, with slopes of ~14 $\mu A*\log(mM)^{-1}$ and ~20 $\mu A*\log(mM)^{-1}$, respectively, for the manual and the fluidic calibrations (Figure S5c). Both linear fittings had R^2 >0.99, indicating a good correlation between concentration and sensor responses. To further evaluate the correlation between the two different experimental approaches, the obtained results for the respective analyte concentration were plotted against each other in Figure S5d. The slope (0.76) of the linear fitting for this plot is close to 1 (slope for perfect correlation), indicating an acceptable agreement between the results obtained using the two experimental approaches. It should be noted that discrepancies between the results might be associated by the different equilibration times between the two experimental approaches, deviations caused by dilution (especially for 1 mM NaCl) and bubble formation that might occur in the microfluidic assisted assay.

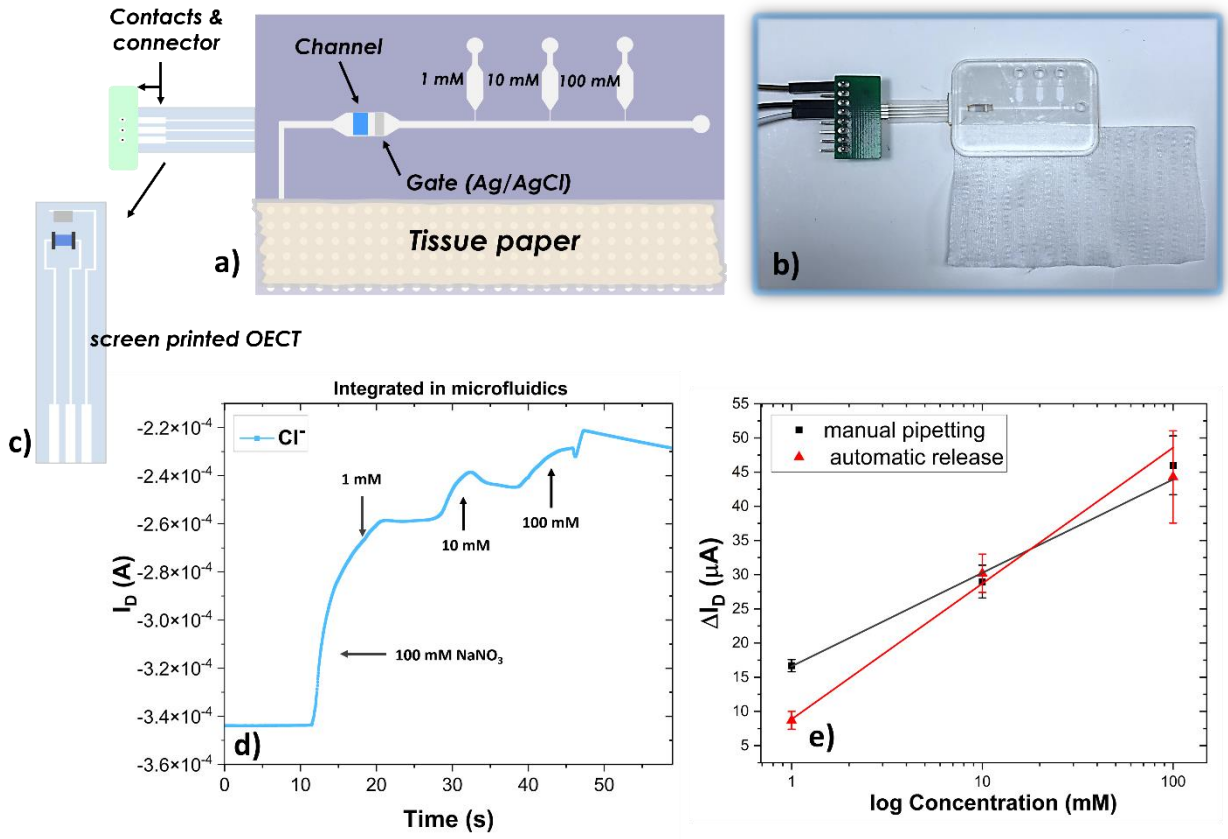

Figure 6. Sensing of Cl^- anions by using the fully screen printed OECT. a) Schematic illustration and b) photograph showing the all-printed embedded with capillary microfluidics and OECT. c) Schematic illustration of an OECT. d) Sensing of Cl^- anions by using an OECT embedded into the microfluidic chip with the automatically released sample solutions reflected on the measurement plot. e) The linear fitting of the current modulation (ΔI_D) as a function of the Cl^- anion concentration.

3. Conclusions

Over the past decades, drop-on-demand inkjet printing of functional materials has allowed lab-on-a-chip (LoC) technology and point-of-care (PoC) diagnostics to evolve from conceptually promising into low cost, disposable, portable and miniaturized tools for medical diagnostics.

The advantages of inkjet printing technology feature fast and low-cost deposition of on-demand shaped coatings in targeted areas, to match complex microfluidic circuits, which in turn modifies the surface chemistry and enables capillary flow in 3DP microfluidics with pre-programmed release of analytes. Additionally, the coatings at the bottom of the channels of the microfluidic circuits also allow for a novel approach of obtaining “stop” and “delay” valves. The inkjet printed coating inside the 3DP microfluidic channels, in contrast with plasma treatment,[10] retains its

surface hydrophilicity for at least 6 months, which indicates its suitability in, *e.g.*, disposable sensor systems. The modified microfluidic circuits were successfully integrated with fully screen printed OECTs to sense and verify the automatic release of multiple test solutions, by current vs. time measurements, inside the 3D-printed microfluidic chip. The initial results confirm the functionality of both the coating in the microfluidic device and the fully printed OECT through the detection of Cl^- anions in the 1-100 mM range in a 100 mM $NaNO_3$ buffer solution.

The results achieved herein pave the way towards the use of printing techniques as a promising tool to enhance and create on-demand surface hydrophilicity in 3D-printed microfluidics, including various geometric patterns that could delay, or even terminate, the fluid flow within the microfluidics. A combination of these tools (inkjet printing and 3D-printing) brings the cost-effectiveness and precision that could shape new microfluidic designs and architectures as well as all-printed sensing platform solutions for PoC and LoC, for the automatic delivery of multiple test solutions and the detection of their ionic species.

4. Experimental section

Fabrication of Microfluidics

The microfluidic devices were designed with SolidWorks 2021 (Dassault Systèmes SE, France) and printed using the stereolithography (SLA) 3D printer Form 3 (Formlabs, USA), laser wavelength of 405 nm, and a 3DP layer thickness of 50 µm. A monocure clear resin (Clear V4 Resin, Formlabs, USA) was used for microfluidic chip fabrication. Post-processing involved cleaning (rinsing with isopropanol, using Formwash, Formlabs, USA) to wash away uncured resin, drying (under a stream of pressurized nitrogen gas), curing (10 minutes under a UV lamp at 60 °C Formcure, Formlabs, USA). The microchannels were 3DP with one open side to avoid trapping resin and reduce over-polymerization. The inkjet printing of the coating was performed into the open side of microchannels, reservoirs, etc.

Fabrication of OECTs

The OECT devices reported here comprise co-planar channels and gate electrodes screen printed on flexible polyethylene terephthalate substrates (PET, 125 µm thick, Polifoil acquired from Policrom Screen). The PET substrates were pretreated at 120 °C for 5 minutes prior fabrication. The manufacturing process was performed by using a DEK Horizon 03iX screen printing

equipment. The device fabrication includes 6 consecutive screen printing steps. Step 1 – printing of Ag-based (Ag 5000 from DuPont) interconnects; step 2 – printing of PEDOT:PSS-based (Clevios S V3, screen printing paste from Hereaus) electrochemically active transistor channels; step 3 – printing of carbon-based (7102 from DuPont) source and drain electrodes; step 4 – printing of PEDOT:PSS-based gate electrodes (Clevios S V3); step 5 – printing of Ag/AgCl electrodes (CI-4025, purchased from Engineered Materials Systems); step 6 – printing of insulator (5018 from DuPont). The steps 1 – 5 require thermal curing at 120 °C for at least 5 minutes, while step 6 requires curing by UV light. The ink/material processing steps are crucial to ensure device functionality.

Sensing of ions (Cl^-) with screen printed OECTs

In the fully screen printed OECT device presented here, the channel and the Ag/AgCl electrode (further employed as the gate electrode) was used for the monitoring of anion (Cl^-) concentration. The respective 1, 10 and 100 mM NaCl solution was prepared in a 100 mM $NaNO_3$ buffer solution, to ensure selectivity upon increasing the anion (Cl^-) concentration.

The sensing of anions (Cl^-) was performed inside the microfluidic system (Figure 6d), thereby including automatic release and delivery of test solutions to the channel and gate electrodes of the OECT.

Coating method

The inkjet printing process was performed by using a Dimatix inkjet printer (DMP – 2800) in ambient conditions. Dimatix SAMBA 10 pL and 2.4 pL cartridges (purchased from Fujifilm) were used. The PSS^-Na^+-based (15 wt%) hydrophilic coating ink was prepared in deionized water and stirred for 2 hours. Further, a high boiling point solvent (polyethylene glycol) was added to achieve a 90:10 wt% ratio. Prior to the inkjet printing process inside the microfluidic channels, a 0.45 µm syringe filter (Acrodisc, PVDF membrane) was used to filter the polyelectrolyte-based ink formulation before filling the cartridge. The printing settings were set to achieve a resolution of 1016 DPI, and several layers were subsequently inkjet printed. The 2.4 and 10 pL cartridges resulted in different coating thicknesses, due to different volumes of the ejected drops. The thicker coatings ensure better wetting properties because of the high surface roughness of the 3DP resin.

For the storage test of 12 days, the coating was stored at ambient conditions (22°C and 47RH%), while the microfluidic devices that were stored for 6 months were kept in a sealed plastic bag.

Embedding 3D-printed microfluidics with OECTs

A laser cutter (Trotec Speedy 300) was used to cut the adhesive tape, according to the shape of the reaction chamber, to ensure a proper contact with the gate electrode and the channel of the OECT, see Figure S6. A double-sided hydrophobic adhesive film (purchased from Paul & Co) was employed to seal the modified microchannels and bond the 3DP microfluidic circuit with the OECT device (Figure S6).

The absorbent pad was attached to the outlet of the microfluidic chip, thereby acting as the capillary pump. Detailed information on the assembly and the stepwise additive manufacturing process of the all-printed sensor system is described in Figure S6 and Figure S7 in the supporting information. The conceptual illustration of the 3DP microfluidic circuit, also including the dimensions of the different parts, *e.g.*, detection site and main channel, is shown in Figure S8. The overall stepwise manufacturing process is further illustrated in Movie S6.

Electrical characterization

All measurements of OECTs embedded into the modified microfluidics were performed under controlled conditions: ~22 °C and ~50 %RH. Electrical characterization (current vs. time measurements) of the OECT devices was carried out using a semiconductor parameter analyzer (HP/Agilent 4155B) to provide voltage to the drain and gate electrodes and to record the drain current vs. time. The drain voltage (V_D) was set to -0.2 or -0.3 V, while various gate voltages were applied (0.2 and 0.4 V) to optimize the drain current modulation.

Supporting Information

Supporting Information is available from the Wiley Online Library or from the author.

Acknowledgements

This project has received funding from the European Union's Horizon 2020 research and innovation programme under the Marie Skłodowska-Curie grant agreement No 813863 (BORGES).

References

[1] A. Olanrewaju, M. Beaugrand, M. Yafia, D. Juncker, *Lab Chip* **2018**, *18*, 2323.

[2] D. Juncker, H. Schmid, U. Drechsler, H. Wolf, M. Wolf, B. Michel, N. de Rooij, E. Delamarche, *Anal. Chem.* **2002**, *74*, 6139.

[3] R. Safavieh, D. Juncker, *Lab Chip* **2013**, *13*, 4180.

[4] A. O. Olanrewaju, A. Robillard, M. Dagher, D. Juncker, *Lab Chip* **2016**, *16*, 3804.

[5] M. Yafia, O. Ymbern, A.O. Olanrewaju, A. Parandakh, A. Sohrabi Kashani, J. Renault, Z. Jin, G. Kim, A. Ng, D. Juncker, *Nature* **2022**, *605*, 464.

[6] A. Parandakh, O. Ymbern, W. Jogia, J. Renault, A. Ng, D. Juncker, *Lab Chip* **2023**, *23*, 6.

[7] B. Zhao, J. S. Moore, D. J. Beebe, *Science* **2001**, *291*, 1023.

[8] B. Zhao, J. S. Moore, D. J. Beebe, *Anal. Chem.* **2002**, *74*, 4259.

[9] P. Lam, K. J. Wynne, G. E. Wnek, *Langmuir* **2002**, *18*, 948.

[10] S. Bouaidat, O. Hansen, H. Bruus, C. Berendsen, N. K. Bau-Madsen, P. Thomsen, A. Wolff, J. Jonsmann, *Lab Chip* **2005**, *5*, 827.

[11] P. Azizian, J. Casals-Terre, J. Ricart, J. M. Cabot, *Analyst* **2023**.

[12] A. Vesel, R. Zaplotnik, M. Mozetič, G. Primc, *Appl. Surf. Sci.* **2021**, *561*.

[13] T. Trantidou, Y. Elani, E. Parsons, O. Ces, *Microsyst. Nanoeng.* **2017**, *3*, 16091.

[14] H. P. Long, C. C. Lai, C. K. Chung, *Surf. Coat. Technol.* **2017**, *320*, 315.

[15] Y. Lu, W. Shi, L. Jiang, J. Qin, B. Lin, *Electrophoresis* **2009**, *30*, 1497.

[16] W. Su, B. S. Cook, Y. Fang, M. M. Tentzeris, *Scientific Reports* **2016**, *6*, 35111.

[17] K. Yamada, T. G. Henares, K, Suzuki, D. Citterio, *Angew. Chem., Int. Ed.* **2015**, *54*, 5294.

[18] A. Prabhu, M. S. G. Nandagopal, P. P. Yegneswaran, H. R. Singhal, N. K. Mani, *Cellulose* **2020**, *27*, 7691.

[19] B. Aghajanloo, F. Ejeian, F. Frascella, S. L. Marasso, M. Cocuzza, A. F. Tehrani, M. H. N. Esfahani, D. W. Inglis, *Lab Chip* **2023**, *23*, 2106.

[20] M. A. U. Khalid, K. H. Kim, A. R. C. Salih, K. Hyun, S. H. Park, B. Kang, A. M. Soomro, M. Ali, Y. Jun, D. Huh, H. Cho, K. H. Choi, *Lab Chip* **2022**, *22*, 1764.

[21] Y. Khan, A. Thielens, S. Muin, J. Ting, C. Baumbauer, A. C. Arias, *Adv. Mater.* **2020**, *32*, 1905279.

[22] P. Calvert, *Chem. Mater.* **2001**, *13*, 3299.

[23] S. Y. Yang, J. A. DeFranco, Y. A. Sylvester, T. J. Gobert, D. J. Macaya, R.M. Owens, G.G. Malliaras, *Lab Chip* **2009**, *9*, 704.

[24] P. Andersson Ersman, R. Lassnig, D. Tu, V. Keshmiri, R. Forchheimer, S. Fabiano, G. Gustafsson, M. Berggren, *Nat. Commun.* **2019**, 10, *5053*.

[25] A. Makhinia, K. Hübscher, V. Beni, P. Andersson Ersman, *Adv. Mater. Technol.* **2022**, *7*, 2200153.

[26] M. Zabihipour, R. Lassnig, J. Strandberg, M. Berggren, S. Fabiano, I. Engquist, P. Andersson Ersman, *npj Flexible Electron.* **2020**, 4, 15.

[27] P. Andersson Ersman, D. Nilsson, J. Kawahara, G. Gustafsson, M. Berggren, *Org. Electron.* **2013**, 14, 1276.

[28] A. M. Pappa, V. F. Curto, M. Braendlein, X. Strakosas, M. J. Donahue, M. Fiocchi, G. G. Malliaras, R. M. Owens, *Adv. Healthcare Mater.* **2016**, *5*, 2295.

[29] P. Lin, X. Luo, I.M. Hsing, F. Yan, *Adv. Mater.* **2011**, *23*, 4035.

[30] X. Ji, H.Y. Lau, X. Ren, B. Peng, P. Zhai, S.P. Feng, P.K.L. Chan, *Adv. Mater. Technol.* **2016**, *1*, 1600042.

[31] J. C. T. Eijkel, A. van den Berg, *Lab Chip* **2006**, *6*, 1405.

[32] S. Ghosh, K. Aggarwal, T. U. Vinitha, T. Nguyen, J. Han, C.H. Ahn, *Microsyst. Nanoeng.* **2020**, *6*, 1.
[33] M. Singh, H. M. Haverinen, P. Dhagat, G. E. Jabbour, *Adv. Mater.* **2010**, *22*, 673.
[34] S. D. Hoath, *Fundamentals of inkjet printing: The science of inkjet and droplets*, Wiley-VCH, Weinheim **2016.**
[35] A. Teichler, R. Eckardt, C. Friebe, J. Perelaer, U.S. Schubert, *Thin Solid Films* **2011**, *519*, 3695.
[36] I. Gualandi, M. Tessarolo, F. Mariani, D. Tonelli, B. Fraboni, E. Scavetta, *Front. Bioeng. Biotechnol.* **2019**, *7*, 354.